Journal of
Nanoscience and Nanotechnology
Vol. 9, 1–6, 2009

Lying-Down Metallic Single-Walled Carbon Nanotubes as Efficient Linkers for Metalloprotein-Based Nanodevices

Chiara Baldacchini† and Salvatore Cannistraro*

Biophysics and Nanoscience Centre and CNISM, Facoltà di Scienze, Università della Tuscia, Largo dell'Università, 01100 Viterbo, Italy

Metalloproteins recently emerged as good candidates for signal transduction in bionanodevices, but the feasibility of such novel devices is strongly connected to the achievement of an efficient charge transport between single metalloproteins and metal electrodes. In this work, we propose the use of metallic single-walled carbon nanotubes as efficient linkers between metalloproteins and metal surfaces. By means of a conductive atomic force microscopy investigation, we compare the conduction across single yeast cytochrome c molecules covalently bound both to bare gold and to functionalized metallic single-walled carbon nanotubes lying on gold. At comparable forces applied by the microscope tip (i.e., comparable physical contact), the measured current is higher when a metallic single-walled carbon nanotubes is in between the metalloprotein and the gold surface. The analysis of the single molecule current responses by means of a non-resonant tunneling transport model suggests that the increasing in the conduction is due both to the strong electronic conjugation existing at the nanotubes/gold interface and to the participation of the nanotube electronic bands to the charge transport.

Keywords: Carbon Nanotubes, Metalloproteins, AFM, Charge Transport, Single Molecule Spectroscopy.

RESEARCH ARTICLE

1. INTRODUCTION

Metalloproteins play a fundamental role in many biological energy transduction processes, owing also to their electron transfer properties, which endow them with charge transport capability spanning over long distances, and in a very fast and directional way. This property, coupled with biorecognition ability, renders metalloproteins promising candidates as basic elements for biosensors at the nanoscale.[1] In such devices, biorecognition events are susceptible to be transduced into electrical signals of low intensity (down to the single electron limit), which could be suitably processed by macroscopic circuits. Charge transport toward the collecting electrodes should takes place across biomolecular chains, involving a subtle balance among non-resonant and resonant tunneling, and hopping processes.[2–5] In order that the external circuits could efficiently collect biorecognition-triggered signals, it is crucial to ensure a good electrical coupling between the bioactive sites and the electrodes. To this aim, the ability of metalloproteins to self-assemble on metal surfaces via specific functional groups can be exploited.[6–10] However, a direct biomolecule–metal interaction could sometimes result too invasive, by inhibiting metalloprotein electron transfer functionality, or even by inducing denaturation.[11,12] Furthermore, direct self-assembly could result in an impairment of the biorecognition ability,[13] as due to a restriction of the biomolecule flexibility, or to a protein orientation hindering the access to the active site. In order to overcome these problems, suitable organic molecules can be used as spacers, connecting metalloproteins and electrodes.[14–18] Specifically designed linkers may help in targeting suitable protein residues, so that the self-assembly can be appropriately driven, controlling, to the desired extent, the strength of the bonding, the orientation of the molecule, and its flexibility.

Among these spacers, single-walled carbon nanotubes (SWNTs) recently emerged as highly attractive candidates.[19,20] due to their low-dimensional character and the corresponding peculiar electronic properties.[21] Moreover, SWNTs are prone to be functionalized by the introduction

*Author to whom correspondence should be addressed.
†Also at INFM-CNR.

on their sidewalls of chemical groups,[22] suitable to target biomolecules with a preferred orientation, also preserving their functionality.[23–25] Nevertheless, to verify if the use of SWNTs as linking spacers is able to implement biodevice performances, a good control of the electrical coupling across the hybrid system is required, and this can be achieved through a deep understanding of the transport mechanisms, which may stem from single molecule conduction characterization.

In this connection, we have investigated the transport properties of single yeast cytochrome c (YCC) molecules covalently bound to functionalized metallic SWNTs (mSWNTs) lying on gold surfaces. The conduction of YCC-mSWNT systems has been measured perpendicularly to the main nanotube axis (Fig. 1(a)), by using an atomic force microscope equipped with a metal coated tip and able to record the electrical current flowing between the tip and the substrate, as a function of the applied bias, at controlled loads (conductive atomic force microscopy: C-AFM). The corresponding current responses, compared with analogous data taken on YCC molecules chemisorbed on bare gold (Fig. 1(b)), and analyzed in the framework of a non-resonant tunneling transport model, are consistent with an increase of the electrical coupling between the metalloprotein and the gold electrode, when connected through the mSWNT.

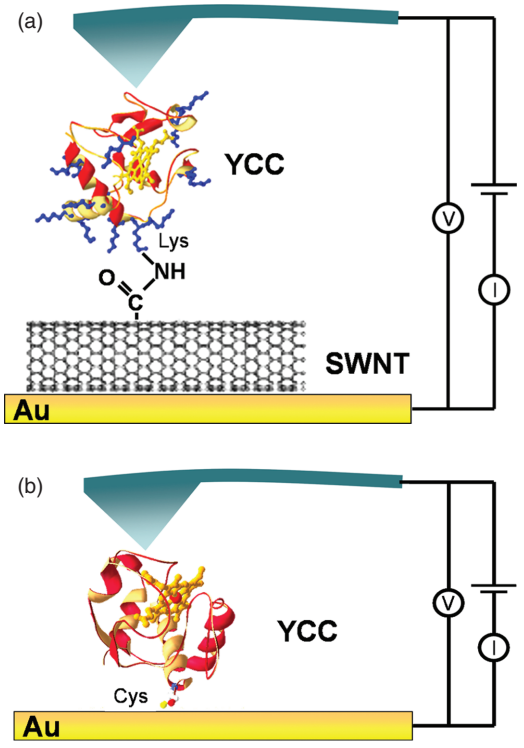

Fig. 1. C-AFM experimental geometries. (a) YCC is anchored to the functionalized mSWNT via an amide bond between a protein lysine and a carboxylic group on the nanotube sidewall, and the mSWNT lies on a gold surface. (b) YCC is covalently immobilized on bare gold through its exposed cysteine.

2. EXPERIMENTAL DETAILS

2.1. Materials

SWNTs (90% pure) and all chemicals and solvents were purchased from Sigma-Aldrich, and used without further purification. The solutions were prepared with ultrapure MilliQ water, obtained by double filtration (Millipore, 18.2 MΩ cm). The substrates consist in 250 nm-thick gold films vacuum-evaporated on boronsilicate glass, supplied by Arrandee™. The gold films were flame-annealed before use, to obtain recrystallized Au(111) terraces hundreds of nanometers wide. The recrystallization of the gold surfaces was checked by means of tapping-mode atomic force microscopy (TM-AFM).

2.2. Sample Preparation

SWNTs were sonicated for 30 minutes in 1,2-dichloethane solution (1 mg/ml), in order to remove bundles, and then dispersed on freshly annealed gold surfaces and dried within 5 minutes in a gentle stream of pure nitrogen. To functionalize them with –COOH groups, the SWNTs adsorbed on gold were etched for less than 1 minute with *piranha* solution (H_2SO_4 (96%): H_2O_2 (30%), 3:1), and then copiously rinsed with MilliQ water. The carboxylic groups at the ends and on the sidewalls of the nanotubes were activated by incubating the samples for 1 hour with a solution of 1-ethyl-3-[3-dimethylaminopropyl]carbodiimide hydrochloride (EDC, 0.5 mg/ml) and *N*-hydroxyl succinimide (NHS, 0.5 mg/ml) in 50 mM sodium phosphate buffer, pH 7. Then, the samples were copiously rinsed with buffer solution and immediately incubated for 1 hour with a 16 μM YCC solution in 50 mM sodium phosphate buffer, pH 7. The excess of unbound proteins was removed by copiously rinse the samples with buffer solution and MilliQ water. The samples were stored in MilliQ water at 277 K until use.

2.3. Tapping-Mode AFM

Measurements were performed in air by using a Nanoscope IIIa/Multimode scanning probe microscope (Digital Instruments), equipped with a 12 μm scanner. Standard silicon cantilevers (RTESP cantilevers, Veeco Probe Centre), with a typical spring constant of about 45 N/m and a tip with nominal radius of curvature of less than 10 nm, were used. The cantilevers were oscillated near their resonance frequency (about 320 kHz), with an oscillation amplitude of about 20 nm. The typical scan rate was 1.0 Hz.

2.4. Raman Spectroscopy

The Raman spectra were collected in air by using a Jobin Yvon LabRAM confocal microspectrometer, and exciting

RESEARCH ARTICLE

with the 632.8 nm radiation line of a HeNe laser 15 mW laser. The microscope (equipped with a 100× objective with NA = 0.9) is confocally coupled to a 300-mm-focal length spectrograph with an 1800 grooves/mm grating (optimized in the red), and the detector is a Peltier-cooled charge coupled device (CCD). Spectral resolution is lower than 5 cm^{-1}.

2.5. Conductive AFM

The measurements were performed in pure nitrogen atmosphere by using a PicoSPM microscope (Molecular Imaging Co.), equipped with a 10 μm scanner and a current sensing module with current sensitivity of 1 nA/V and an operational range between few pA and 10 nA. Standard silicon cantilevers coated with a platinum film (NSC36/Pt cantilevers, Mikromash), with typical spring constant of 0.6 N/m and nominal tip radius of curvature less than 25 nm were used. Each *I–V* curve was acquired at a fixed applied load on a single protein, by mediating on 20 consecutive bias sweeps. Each bias sweep was registered in 0.4 s and, since the overall drift in the *x–y* plane was evaluated to be less than 1 Å/s, the shift of the tip position during the acquisition is negligible (1% of the protein lateral size).

3. RESULTS AND DISCUSSION

3.1. Morphology

Representative TM-AFM images and Raman spectra of pure and functionalized SWNTs on a gold surface are shown in Figure 2. Pure SWNTs appear clean, unbundled, and with a length of several hundred nanometers (Fig. 2(a)), and their Raman spectrum presents a dominant G band at about 1570 cm^{-1} and a weaker D band at about 1320 cm^{-1} (Fig. 2(b)), as expected.[26] Once treated with the "piranha" solution, the nanotubes are shortened (100–200 nm) and clear defects are introduced at their ends (Fig. 2(c)), and the D band intensity in the Raman spectra is strongly increased (Fig. 2(d)), indicating the formation of the functional groups.[27] On the contrary, the gold surface results unchanged if checked by means of both TM-AFM and Raman spectroscopy. After the activation of the carboxylic groups, the SWNTs adsorbed on gold were incubated with an YCC solution, and representative TM-AFM images of the resulting surface are shown in Figures 2(e, f). The metal surface is covered by a compact layer of globular objects (with a texture recalling that observed for a monolayer of YCC molecules chemisorbed on gold[8]), while a SWNT appears decorated by bumps with a mean height of about 4.0 nm (which are reminiscent of cytochrome c molecules coating nanotubes[23, 28]). The bigger bumps observed (7–12 nm) are likely due to impurities or protein aggregates.

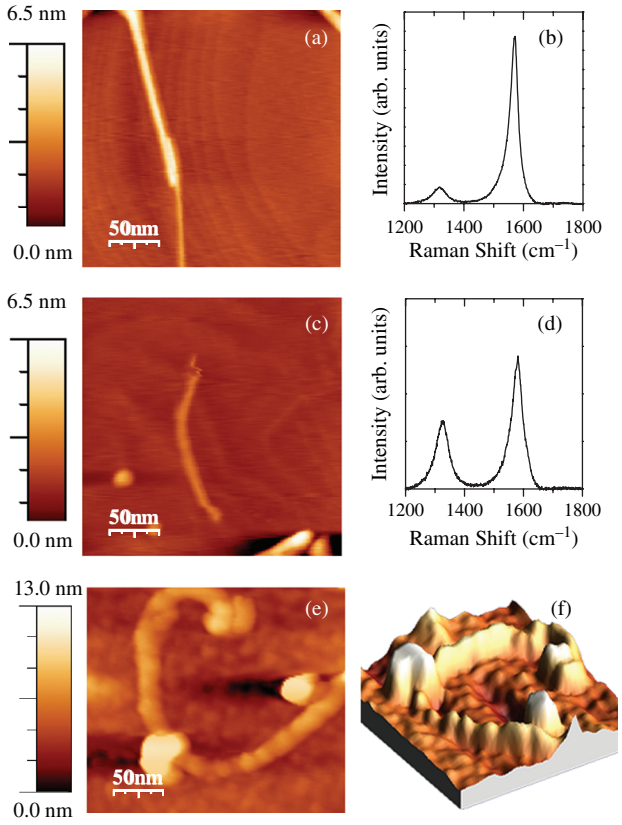

Fig. 2. Bounding YCC molecules to SWNTs. (a) Representative TM-AFM image of pure SWNTs on a gold surface. (b) Representative Raman spectrum of pure SWNTs on a gold surface. (c) Representative TM-AFM image of a SWNT on gold after the oxidative treatment. (d) Representative Raman spectrum of SWNTs on gold after the oxidative treatment. (e, f) Representative TM-AFM image of a SWNT with chemisorbed YCC molecules shown in two- and three-dimensions.

3.2. Conduction Properties

The conduction properties of single YCC molecules bound both to bare gold and to SWNTs were characterized by means of C-AFM. This technique allows the topography and the current response of a sample to be mapped simultaneously, by scanning the surface with a metal coated tip in contact-mode AFM, while a fixed bias is applied between the tip and the substrate. Moreover, by setting the tip position and the contact force, the current response of the sample can be recorded as a function of the applied bias (*I–V* curves). SWNTs were first located on the surface by means of topographic imaging, while the corresponding current images allowed discriminating metallic from semiconducting nanotubes.[29] Then, *I–V* curves were collected by positioning the conductive tip on top of a protein molecule adsorbed on a mSWNT (accordingly to the geometry depicted in Fig. 1(a)), at different contact forces. For comparison, analogous measurements were performed on the nearby YCC molecules bound to bare gold (see Fig. 1(b)).

RESEARCH ARTICLE

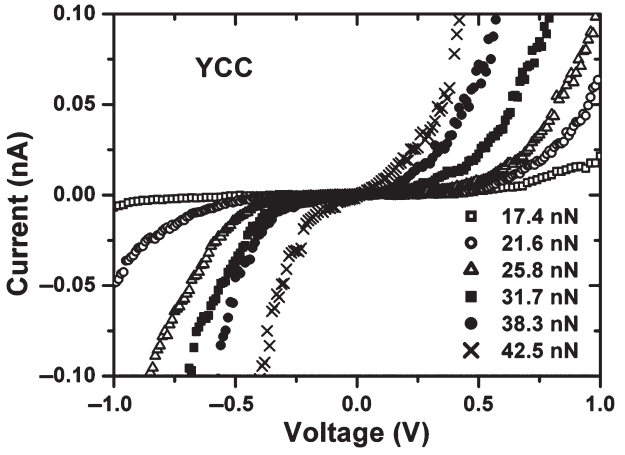

Fig. 3. *I–V* characteristics of an YCC molecule chemisorbed at a gold surface, at different applied forces, as obtained by mediating on the current response of several proteins.

Typical *I–V* curves recorded on YCC molecules bound to bare gold and to a mSWNT are shown in Figures 3 and 4, respectively. The *I–V* characteristics of both systems display an almost sigmoidal shape within the range of applied bias (±1 V). For YCC molecules bound to bare gold, the current response monotonically increases with raising the load (Fig. 3). For instance, at a bias of 0.45 V the current signal increases of almost two orders of magnitude (from about 1 to 100 pA), when the applied force is more than doubled (from 17.1 to 42.5 nN). It turns out that, in the same range of forces, the resistance decreases from 1.0×10^{12} to 1.4×10^{10} Ω, as estimated by linearly fitting the current curves around zero bias. Such behavior has been observed for other metalloproteins adsorbed on bare conductive surfaces.[10, 30, 31] Being commonly assumed that a stable electrical contact is established once a significant current signal is recorded, the resistance variation has been associated either to a larger number of molecules

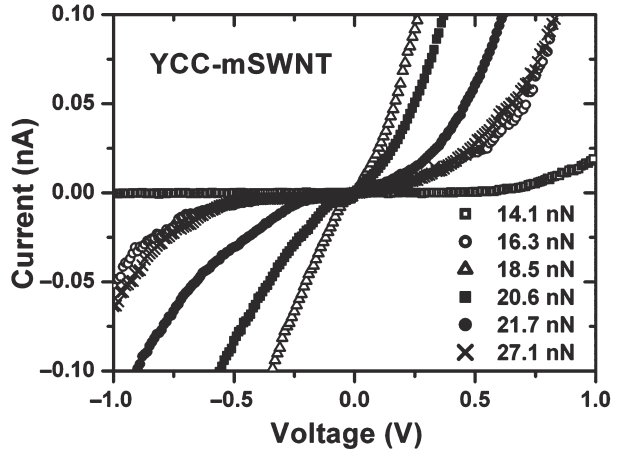

Fig. 4. *I–V* characteristics of an YCC molecule covalently bound to a metallic SWNT lying on a gold surface, recorded at different applied forces.

contacted with varying the pressure, or to the molecular deformation under mechanical stress.[10, 30, 31]

A representative current response for the YCC-mSWNT system is shown in Figure 4. It exhibits a rapid increase, by raising the applied load from 14 to about 19 nN, and then it decreases at higher forces. For instance, at an applied bias of 0.45 V, an initial 35% increment in the applied load determines a current rising from about 1 to 200 pA, while a further increase of the applied force induces a current drop, down to 20 pA. Interestingly, currents as high as 200 pA, corresponding to resistances as low as 4.0×10^9 Ω, are higher than any current we measured across YCC molecules directly bound to gold (for applied forces in the 17–42 nN range), despite the larger tip-to-gold substrate distance (as due to the presence of the nanotube). Owing to the non univocal orientation of the proteins (several lysine residues are present on the protein shell) and to the non uniform distribution of the SWNT diameters, the current data we collected on YCC-mSWNT systems are quantitatively scattered. However, the trend of the current as a function of the applied load (reaching a maximum value in the 10^2 pA range at about 20 ± 2 nN of applied force) is a peculiarity observed for every YCC-mSWNT system studied. Such a non-monotonic current dependence on the applied load is strongly reminiscent of the peculiar transverse current response of bare metallic SWNTs on gold surfaces, which is due to the activation of band-like conduction mechanisms at loads of about 20 nN.[29] Thus, even if we never observed analogous ohmic-like conduction across an YCC-mSWNT system (as due to the presence of the intrinsically dielectric protein), these results suggest that the delocalized electronic bands of the mSWNTs are directly involved in the conduction measurements we performed across the YCC-mSWNT systems.

To get a deeper insight on this aspect, the *I–V* curves collected on YCC molecules bound both to bare gold and to mSWNTs have been analyzed within the framework of a tunneling transport model. The conduction through a redox protein is due to a delicate balance between resonant and non-resonant tunneling. Resonant tunneling should give rise to negative differential resistances (NDRs) in the *I–V* curves,[32, 33] but we did not observe any NDR in the investigated range of applied bias (±1 V) and forces (14–40 nN). Indeed, for redox proteins, NDRs generally occur at higher applied bias,[32, 33] and only at applied forces as low as for STM-like condition (i.e., lower than 5 nN).[32] Since we worked at applied loads higher than 10 nN, in order to establish a good electrical contact, we can assume that non-resonant tunneling dominates the transport. Thus, the model we applied is based on the Landauer approach, which describes the current across a molecule between two electrodes as flowing through a one-dimensional channel,[4] and, by considering only non-resonant tunneling, the molecular medium is treated as a continuum barrier. The current results to be proportional to the quantum of conductance G_0 and to the tunneling transmission probability

$T = e^{-\beta L}$, where L is the tunneling barrier length and $\beta = (4\pi/h)(2m\alpha(H - \mathrm{eV}/2))^{1/2}$ is the tunneling decay parameter (with h the Plank constant, m the effective electron mass assumed to be 0.16 m_e, H the barrier height, V the bias between the electrodes, and α a parameter ranging between 0 and 1, which describes how symmetric the contacts with the electrodes are).[4, 34] Accordingly, the I–V curves were fitted with the formula $I = AG_0e^{-\beta L}V$, where A is a term taking into account the transmission probabilities at the contact points, assumed to be constant at those loads at which a non negligible current is recorded.[34, 35] Analogous models have been previously used in the interpretation of I–V curves measured on organic molecule[34] or protein[30–32, 35] monolayers.

Representative best fits of I–V curves are shown in Figures 5(a and b), one for each investigated system. From the fitting procedure, we may extract the tunneling barrier length L and height H, and the parameter α. At the lowest applied loads, L results to be consistent with the physical dimensions (3.0 nm for the YCC molecule and 3.5 nm for the YCC-mSWNT system), and it slightly decreases with increasing the applied force, as previously observed.[29–31, 35] For YCC molecules on bare gold, H decreases with raising the load (from about 1.0 to about 0.7 eV), assuming values consistent with those previously reported in the literature: at an applied load of about 32 nN, H is about 0.85 eV for YCC molecules on gold, while the barrier heights of YCC and azurin molecules on graphite were found to be about 1.00 and 0.71 eV, respectively.[30, 31] On the contrary, for the YCC-mSWNT system, H first decreases and then increases, with a minimum value of about 0.5–0.4 eV at applied forces in the 15–22 nN range. Finally, the parameter α describes the symmetry of the electrical contacts between the molecular system and the electrodes. For YCC molecules on bare gold, α is found to be about 1, indicating that the protein electrical coupling with both the electrodes is similar (as previously observed for azurin,[30] plastocyanin,[35] and YCC itself[31]), while for the YCC-mSWNT system, α is found to be about 0.4, suggesting that the electrical contact at the mSWNT-gold interface is different from that between the tip and the YCC molecule on top of the nanotube. In particular, since a more efficient conduction is observed for this system, we may infer that a higher electrical coupling resides at the mSWNTs-gold interface, with respect to the tip-to-protein contact. Indeed, it has been recently shown that lying-down carbon nanotubes strongly interacts with metal surfaces,[36] due to a wide electronic coupling (i.e., hybridization) between the nanotube molecular orbitals and the gold surface electronic states.[37]

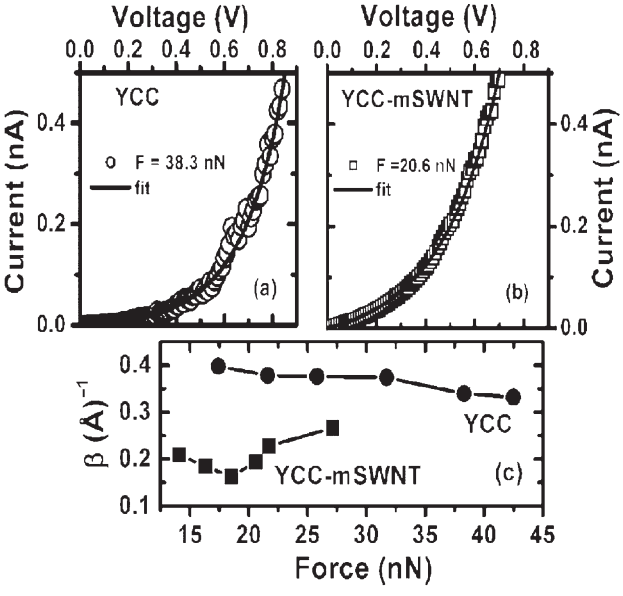

Fig. 5. Application of the tunneling transport model and fitting results. (a) Best fitting curve of the positive bias region of the I–V characteristic of an YCC molecule on bare gold. (b) Best fitting curve of the positive bias region of the I–V characteristic of an YCC-mSWNT system. (c) Evolution of the tunneling decay parameter as a function of the applied force, as obtained by fitting the curves in Figures 3 and 4.

Once H and α have been obtained from the fitting procedure, by assuming $V = 0$, the tunneling decay parameter β can be calculated. It describes the tunneling conduction efficiency across the molecular milieu, and the lower its value, the higher the electronic coupling of the system is. For instance, β is about 1 Å^{-1} in alkane chains, while it ranges between 0.6 and 0.2 Å^{-1} for π-conjugated systems, and it is expected to be as low as 0.1 Å^{-1} for unsaturated or delocalized systems.[34, 38] Figure 5(c) shows the β trends as a function of the applied loads, as obtained by fitting the I–V curves in Figures 3 and 4. For YCC molecules adsorbed on bare gold, β is found to vary from 0.40 to 0.33 Å^{-1}, confirming that the conduction across the protein is mainly due to non-resonant electron tunneling.[34] On the contrary, for the YCC-mSWNT system, the tunneling decay parameter is lower than 0.20 Å^{-1} up to an applied force of about 22 nN, indicating that a transport mechanism more efficient than electron tunneling is responsible for the charge transport in this range of applied forces. At higher applied loads, the conduction switches into a tunneling regime, as previously observed for bare mSWNTs,[29] where the induced nanotube deformation avoids band-like transport.

4. CONCLUSIONS

We performed the first single-molecule C-AFM measurement on metalloproteins bound to mSWNTs lying on gold surfaces. Our results show that the charge transport is more efficient across the YCC-mSWNT system than across an YCC molecule directly bound to gold. This can be due to both a higher functionality preservation of the protein, and to an improvement of the electrical coupling between the protein and the metal surface, due to the presence of the mSWNTs used as linking spacer. Indeed, the analysis of

RESEARCH ARTICLE

the I–V data within the framework of a non-resonant tunneling transport model reveals that the mSWNTs enhance both the electrical conjugation at the interface with the gold electrode and the transport efficiency across the molecular milieu. Thus, the present study points out that lying-down mSWNTs, used as linking spacers, may pave the way to the development of new nanotube-based biodevice architectures.

Acknowledgment: This research was partially funded by the PRIN-MIUR Research Project (Grant No. 2006028219). We are grateful to Dr. Laura Andolfi and to Professor Anna Rita Bizzarri for useful discussions.

References and Notes

1. B. Willner, E. Katz, and I. Willner, *Curr. Opin. Biotechnol.* 17, 589 (**2006**).
2. S. Datta, Electronic Transport in Mesoscopic Systems, Cambridge University Press, Cambridge (**2001**).
3. J. Chen, T. Lee, J. Su, W. Wang, and M. A. Reed, Encyclopaedia of Nanoscience and Nanotechnology, American Scientific Publishers, Los Angeles (**2004**), p. 1.
4. S. Lindsay, *J. Chem. Educ.* 82, 727 (**2005**).
5. A. R. Bizzarri and S. Cannistraro, Encyclopaedia of Condensed Matter Physics, edited by G. Bassani, G. Liedl, and P. Wyder, Elsevier, Amsterdam (**2005**), p. 361.
6. J. J. Davis, D. Djuricic, K. K. W. Lo, E. N. K. Fallace, L.-L. Wong, and H. A. O. Hill, *Faraday Discuss.* 116, 15 (**2000**).
7. Q. Chi, J. Zhang, J. U. Nielsen, E. P. Friis, I. Chorkendorff, G. W. Canters, J. E. T. Andersen, and J. Ulstrup, *J. Am. Chem. Soc.* 122, 4047 (**2000**).
8. B. Bonanni, D. Alliata, A. R. Bizzarri, and S. Cannistraro, *ChemPhysChem.* 4, 1183 (**2003**).
9. L. Andolfi, D. Bruce, S. Cannistraro, G. W. Canters, J. J. Davis, H. A. O. Hill, J. Crozier, M. Ph. Verbeet, C. L. Wrathmell, and Y. Astier, *J. Electroanal. Chem.* 565, 21 (**2004**).
10. L. Andolfi and S. Cannistraro, *Surf. Sci.* 598, 68 (**2005**).
11. Y. Zhou, T. Nagaoka, and G. Zhu, *Biophys. Chem.* 79, 55 (**1999**).
12. D. L. Johnson, C. J. Maxwell, D. Losic, J. G. Shapter, and L. L. Martin, *Bioelectrochem.* 58, 137 (**2002**).
13. B. Bonanni, A. R. Bizzarri, and S. Cannistraro, *J. Phys. Chem. B* 110, 14574 (**2006**).
14. M. J. Tarlov and E. F. Bowden, *J. Am. Chem. Soc.* 113, 1847 (**1991**).
15. Q. Chi, J. Zhang, J. E. T. Andersen, and J. Ulstrup, *J. Phys. Chem. B* 105, 4669 (**2001**).
16. X. Chen, R. Ferrigno, J. Yang, and G. M. Whitesides, *Langmuir* 18, 7009 (**2002**).
17. J. Liu, M. N. Paddon-Row, and J. J. Gooding, *J. Phys. Chem. B* 108, 8460 (**2004**).
18. I. Delfino, B. Bonanni, L. Andolfi, C. Baldacchini, A. R. Bizzarri, and S. Cannistraro, *J. Phys.: Condens. Matter* 19, 225009 (**2007**).
19. E. Katz and I. Willner, *ChemPhysChem.* 5, 1084 (**2004**).
20. G. Gruner, *Anal. Bioanal. Chem.* 384, 322 (**2006**).
21. Ph. Avouris, Z. Chen, and V. Perebeinos, *Nature Nanotech.* 2, 605 (**2007**).
22. D. Tasis, N. Tagmatarchis, V. Georgakilas, and M. Prato, *Chem. Eur. J.* 9, 4000 (**2003**).
23. B. R. Azamian, J. J. Davis, K. S. Coleman, C. B. Bagshaw, and M. L. H. Green, *J. Am. Chem. Soc.* 124, 12664 (**2002**).
24. J. J. Gooding, R. Wibowo, J. Liu, W. Yang, D. Losic, S. Orbons, F. J. Mearns, J. G. Shapter, and D. B. Hibbert, *J. Am. Chem. Soc.* 125, 9006 (**2003**).
25. J. Liu, A. Chou, W. Rahmat, M. N. Paddon-Row, and J. J. Gooding, *Electroanalysis* 17, 38 (**2005**).
26. M. S. Dresselhaus, G. Dresselhaus, A. Jorio, A. G. Souza Filho, and R. Saito, *Carbon* 40, 2043 (**2002**).
27. P. C. Eklund, J. M. Holden, and R. A. Jishi, *Carbon* 33, 959 (**1995**).
28. S. Boussaad, N. J. Tao, R. Zhang, T. Hopson, and L. A. Nagahara, *Chem. Comm.* 1502 (**2003**).
29. C. Baldacchini and S. Cannistraro, *Appl. Phys. Lett.* 91, 122103 (**2007**).
30. J. Zhao, J. J. Davis, M. S. P. Sansom, and H. Andrew, *J. Am. Chem. Soc.* 126, 5601 (**2004**).
31. D. N. Axford and J. J. Davis, *Nanotechnology* 18, 145502 (**2007**).
32. D. Axford, J. J. Davis, N. Wang, D. Wang, T. Zhang, J. Zhao, and B. Peters, *J. Phys. Chem. B* 111, 9062 (**2007**).
33. Q. Tang, H. K. Moon, Y. Lee, S. M. Yoon, H. J. Song, H. Lim, and H. C. Choi, *J. Am. Chem. Soc.* 129, 11018 (**2007**).
34. A. Salomon, D. Cahen, S. Lindsay, J. Tomfohr, V. B. Engelkes, and C. D. Frisbie, *Adv. Mater.* 15, 1881 (**2003**).
35. L. Andolfi, A. R. Bizzarri, and S. Cannistraro, *Appl. Phys. Lett.* 89, 183125 (**2006**).
36. T. Hertel, R. Martel, and Ph. Avouris, *J. Phys. Chem. B* 102, 910 (**1998**).
37. Y. Xue and S. Datta, *Phys. Rev. Lett.* 83, 4844 (**1999**).
38. J. J. Davis, *Phil. Trans. R. Soc. Lond. A* 361, 2807 (**2003**).

Received: 10 December 2008. Accepted: 20 January 2009.